

Seeking the nearest neutron stars using a new local electron density map

Joseph Bramante,^{a,b,c} Katherine Mack,^c Nirmal Raj,^e Lijing Shao,^{f,g} Narayani Tyagi^{a,b,1}

^aDepartment of Physics, Engineering Physics, and Astronomy, Queen’s University, Kingston, Ontario, K7N 3N6, Canada

^bThe Arthur B. McDonald Canadian Astroparticle Physics Research Institute, Kingston, Ontario, K7L 3N6, Canada

^cPerimeter Institute for Theoretical Physics, Waterloo, Ontario, N2L 2Y5, Canada

^eCentre for High Energy Physics, Indian Institute of Science, C.V. Raman Avenue, Bengaluru 560012, India

^fKavli Institute for Astronomy and Astrophysics, Peking University, Beijing 100871, China

^gNational Astronomical Observatories, Chinese Academy of Sciences, Beijing 100012, China

E-mail: joseph.bramante@queensu.ca, kmack@perimeterinstitute.ca,
nraj@iisc.ac.in, lshao@pku.edu.cn, narayani.tyagi@queensu.ca

Abstract. Neutron stars provide a compelling testing ground for gravity, nuclear dynamics, and physics beyond the Standard Model, and so it will be useful to locate the neutron stars nearest to Earth. To that end, we revisit pulsar distance estimates extracted from the dispersion measure of pulsar radio waves scattering on electrons. In particular, we create a new electron density map for the local kiloparsec by fitting to *parallax* measurements of the nearest pulsars, which complements existing maps that are fit on the Galactic scale. This “near-Earth” electron density map implies that pulsars previously estimated to be 100–200 pc away may be as close as tens of parsecs away, which motivates a parallax-based measurement campaign to follow-up on these very-near candidate pulsars. Such nearby neutron stars would be valuable laboratories for testing fundamental physics phenomena, including several late-stage neutron star heating mechanisms, using current and forthcoming telescopes. We illustrate this by estimating the sensitivities of the upcoming Extremely Large Telescope and Thirty Meter Telescope to neutron stars heated by dark matter capture.

¹Corresponding author

Contents

1	Introduction	1
2	Review of electron density models	3
2.1	NE2001	3
2.2	YMW16	3
2.3	Limitations of existing models	4
3	A new local kiloparsec electron density map	5
3.1	The importance of parallax measurements	5
3.2	Parallax-fitted local electron distribution	5
4	Prospects for observing dark matter-induced neutron star reheating	8
4.1	Review of dark kinetic and annihilation heating	8
4.2	Measuring neutron star temperatures with TMT and ELT	9
5	Conclusion	10
Appendices		12
A	Pulsar properties	12
B	Modified electron density map in galactocentric representation	14

1 Introduction

How near is the nearest neutron star to Earth? Answering this question accurately may have far-reaching implications for fundamental physics and astrophysics, since neutron stars (NSs) constitute some of their most sensitive laboratories [1–3]. For example, precise measurements of the masses and radii of nearby NSs would be essential to constrain the state equation of high-density matter [4], and their velocities would help pinpoint their kinematic age [5], all of which would sharpen our understanding of passive cooling of NSs [6–8]. Of particular interest to us in this regard are the late-stage reheating mechanisms of NSs, such as numerous heating mechanisms involving a hidden sector of particles [2], including dark matter and other proposed astrophysical effects [9]. For recent reviews of hidden sector and astrophysical mechanisms, see *e.g.* Ref. [2] and the Appendix of Ref. [10].

Only about 5–10% of NSs are observed as radio pulsars, primarily due to their beam orientation, brightness, and distance limitations. Including x-ray and gamma-ray observations, the observable fraction might be closer to 10% [11]. The closest known pulsar is estimated to be 110–130 pc away [12, 13], whereas from the number density of NSs in the solar vicinity, $n_{\odot} \simeq (1 - 5) \times 10^{-4} \text{pc}^{-3}$ (assuming 10^9 NSs in the Galaxy) [14, 15], we obtain a theoretical distance to the nearest NS of only $(3/4\pi n_{\odot})^{1/3} \simeq 10$ pc. This calls for a close scrutiny of the region around us. Of course, the spatial pulsar distribution in our galaxy has been a topic of interest for a few decades now. Thanks to the current generation of large-scale pulsar surveys [16–23], we now have large samples of both regular ($\mathcal{O}(1)$ s period) and millisecond pulsars. Along with the ATNF pulsar catalogue [16], which is considered the standard, other

databases such as the EPN database of pulsar profiles [23] and the Green Bank North Celestial Cap (GBNCC) pulsar survey [17–22], provide detailed accounts of discovered pulsars.

Pulsar distance estimates in these catalogues are often based on radio pulsar dispersion measures (DMs), which in turn rely on two prominent models that map the Galactic free-electron distribution: NE2001 [24] and YMW16 [25]. Combined with direct measurements of a pulsar’s radio DMs, these can be used to estimate distances to pulsars in the Milky Way. These models have been well-calibrated to achieve remarkable precision on distance scales of kiloparsecs (kpc) and above with YMW16 a significant refinement of the earlier NE2001. Both models integrate an array of Galactic features, including spiral arms, thin and thick disks, and localized clumps of electron density, allowing for an accurate reconstruction of the interstellar medium (ISM) structure. As such, for pulsar timing arrays, studies of the interstellar medium, and efforts to probe Galactic structure, the YMW16 and NE2001 models prove indispensable for finding distances across vast galactic distances. However, both models have some drawbacks, especially when it comes to accurately predicting distances to nearby pulsars, due to large uncertainties in estimates of the *local* free-electron density in the 1 kpc vicinity of the Sun. Upon close inspection of pulsars with distances given by radio parallaxes, these models appear not to account for severe overdensities and underdensities of electrons in this region. This is a point conceded by YMW16 in Ref. [25], where it is stated that this loss of accuracy is an unavoidable consequence of its inability to adequately model small-scale structure.

In this work, we formulate a new simplified free electron density map as an aid to finding the closest pulsar. We calibrate this map using *parallax* measurements of pulsar distances within 1 kpc of Earth, as these measurements are generally known to be reliable. With our simplified map, we predict and list the distances of several promising pulsar candidates. Using this method, we find some candidate nearest NSs *already discovered in the sky* that may be only a few tens of parsecs away. If any of these candidate nearby NSs are confirmed by future parallax measurement, they may provide a valuable new target for testing NS properties, and especially late-stage heating. In the latter half of this article we illustrate this utility by studying nearby NS sensitivity for a minimal mechanism arising from dark matter: kinetic heating of NSs [26], possibly augmented by self-annihilations in their interior. We will assume two benchmark temperatures resulting from dark kinetic heating: 2500 K and 10000 K, the latter of which is possible if dark matter is clumped in microhalos [27]. These are below the upper bound on the coldest NS observed thus far, about 30000 K [28], and may be measured by the James Webb Space Telescope (JWST), the Thirty Meter Telescope (TMT), or the Extremely Large Telescope (ELT). Using Exposure Time Calculators available online,¹ we estimate the distances to reheated NSs that would be within the sensitivity of the future TMT and ELT, for reasonable exposure times.

This paper is organized as follows. In Section 2 we review the electron density models NE2001 and YMW16, and discuss their advantages and disadvantages. In Section 3 we present our simplified electron density model, valid only for the solar vicinity, and use it to revise the dispersion measure distance estimates to nearby pulsars. In Section 4 we review dark kinetic heating and forecast the observational limits obtainable by TMT and ELT to demonstrate the immediate use of our main results. In the Appendix, we provide a detailed list of the closest pulsar candidates identified through our simplified map, including potential binary companions identified in the Gaia database, along with their revised distance estimates.

¹www.tmt.org/etc/iris, www.eso.org/observing/etc

2 Review of electron density models

In pulsar astronomy, the DM is a key observable that quantifies the total column density of free electrons between the observer and a pulsar along the line of sight:

$$\text{DM} = \int_0^L n_e(\ell) d\ell, \quad (2.1)$$

where L is the distance along the line of sight and n_e is the electron number density [29]. The lower frequency waves of a radio pulse arrive later than the higher frequency waves due to dispersion by the ISM.

The delay in arrival times of waves with frequencies f_1 and f_2 is then given by

$$\Delta t \propto \text{DM} \left(\frac{1}{f_1^2} - \frac{1}{f_2^2} \right). \quad (2.2)$$

Using Δt measurements for various lines of sight and pulse frequencies, combined with distance estimates, the spatial distribution of free electrons in the galaxy may be modeled.

This method has produced empirical electron density maps for the Milky Way, but since there may be small non-electron contributions to the DM, it has been recently advocated [30] that the directly measured quantity $\mathcal{D} \equiv \Delta t (f_1^{-2} - f_2^{-2})^{-1}$ be reported by astronomers instead of the DM inferred from Eq. (2.2).

Over the past decades several models have been developed to create and refine these maps, the most notable of which we will now briefly describe.

2.1 NE2001

The NE2001 model [24], making use of measurements of pulsar DM and distances and radio-wave scattering, built upon and superseded the 1993 model of Taylor and Cordes (TC93) [31] for the Galactic distribution of free electrons.

The basic structure consists of three smooth components – thick disk, thin disk, and spiral arms –, the Galactic Center, the local ISM, clumps, and voids. The NE2001 model calculates the local electron density by blending contributions from different regions of the Galaxy, each with its own distinct properties. The model begins by considering the primary electron sources, the Galactic disk and the Galactic Center, which dominate the electron density. It then accounts for the influence of the ISM and further introduces corrections for voids—regions with low electron density—and denser clumps of electrons scattered throughout the Galaxy. By assigning weights to these components, the model ensures that the distribution reflects their varying levels of influence. This weighting allows for a more nuanced and accurate representation of the electron density, especially across diverse environments within the Milky Way.

2.2 YMW16

The YMW16 model [25] predicts the large scale distribution of free electrons in the Galaxy, Large Magellanic Cloud (LMC), Small Magellanic Cloud (SMC), and the Intergalactic Medium (IGM). The Galactic part of this model follows the same basic structure as NE2001, with the addition of a four-armed spiral pattern along with a local arm, the location and form of the arms based on observations of > 1800 H-II regions across the Galaxy. This model is then fitted to 189 independent estimates of pulsar distances that make use of parallaxes, Galactic

rotation kinematics of H-I clouds with absorption features, and association with other celestial objects.

Key features in YMW16 (most of which were also part of NE2001) are: the Local Bubble, two regions of enhanced electron density on the periphery of the Local Bubble, the Gum Nebula, a region of enhanced electron density in the Carina arm, and a region of reduced electron density in the tangential periphery of Sagittarius. One major difference between NE2001 and YMW16 is the modeling of the large scale distribution of interstellar scattering: NE2001 incorporates this effect, while YMW16 omits it. This is because numerous studies have demonstrated that interstellar scattering is often dominated by only a few regions, with significant electron density fluctuations along the path to a pulsar, making it complicated to model. Another salient difference is that YMW16 does not incorporate clumps and voids to rectify discrepant model distances to some pulsars, in order to avoid future discrepancies for pulsars that may yet be discovered close to their lines of sight.

DM pulsar distance estimates in the ATNF catalogue [16] use the YMW16 model as default. However, other distance estimates can improve accuracy. For example, distances determined by association with another object, such as the LMC or a supernova remnant, and those based on measured annual parallax (with an uncertainty less than one-third of the parallax value) are generally more reliable than distances derived from DMs. For the Local Bubble, there is reason to believe that there is a non-linear relationship between the DMs and the distances, (see Eq. (2.1)) since we expect inhomogeneities in the local ISM electron density [32].

2.3 Limitations of existing models

Both the leading electron density maps have some limitations. The NE2001 model has large errors in distance estimates within 1 kpc of Earth, as this model was initially designed with regard to the overall structure of the Galaxy as opposed to fine features of the local region around the Solar neighborhood. For instance, while the YMW16 model predicts a distance of 143 pc for pulsar J0536–7543 based on the DM, NE2001 places it at 826 pc. This discrepancy highlights the NE2001 model’s broader focus on the large-scale Galactic structure, which can lead to substantial errors when estimating distances in the local region around Earth. Further discrepancies arise due to assumptions about local electron density variations that are ill-constrained due to the sparse pulsar DM observations available at the time of inception of this model. While the model incorporates several large scale galactic features, it doesn’t give an accurate representation for smaller scale structure, which significantly impact DM interpretation for nearby pulsars.

The YMW16 model utilizes more recent observational data, including several parallax measurements for a more extensive pulsar database, but still falls short when it comes to accurately describing the local free electron density. This is due to the fact that while the model refines the large scale features, this does not always translate to a higher precision for nearby pulsars, where small scale variations are more pronounced. Both NE2001 and YMW16 contain simplifications that can introduce systematic errors for nearby pulsar distance estimates. These include assuming a smooth distribution of electrons and not accounting for small-scale clumpiness or voids in the ISM.

3 A new local kiloparsec electron density map

3.1 The importance of parallax measurements

Pulsar distances are measured most robustly with parallax methods that use pulsar timing to localize their sky position [33, 34] and/or very long baseline interferometry (VLBI) [35, 36]. A significant discrepancy between the VLBI-derived distances and those estimated from DM measurements combined with the NE2001 and YMW16 models was noted for 57 pulsars [35]. As noted in Ref. [10], PSR J1057–5226 is estimated to be at 93 pc by the YMW16 model and listed as the closest pulsar in the ATNF catalogue, but is estimated to be 730 ± 150 pc away by the NE2001 model and 1530 pc away by the TC93 model [37]. Moreover, an analysis of the optical and x-ray spectrum [38] puts PSR J1057–5226 at 350 ± 150 pc. To our knowledge, no parallax measurement of its distance has been undertaken.

Such discrepancies arise due to inherent limitations and systematics of the DM method. This is quantified in the YMW16 model [25] by the statement that it comes with a less-than-90% uncertainty on 95% of its distance estimates. Note that typical uncertainties in parallax distance estimates are 10%–20%, underscoring their importance for not only pulsar distances but also the ISM distribution. And as already noted, previous electron density models are unreliable on sub-kpc scales – and it is exactly in the local $\mathcal{O}(\text{kpc})$ region that parallax measurements work best. Accurate distances to neighboring pulsars are, we re-emphasize, crucial for various astrophysical studies such as that of dark matter interactions with NSs.

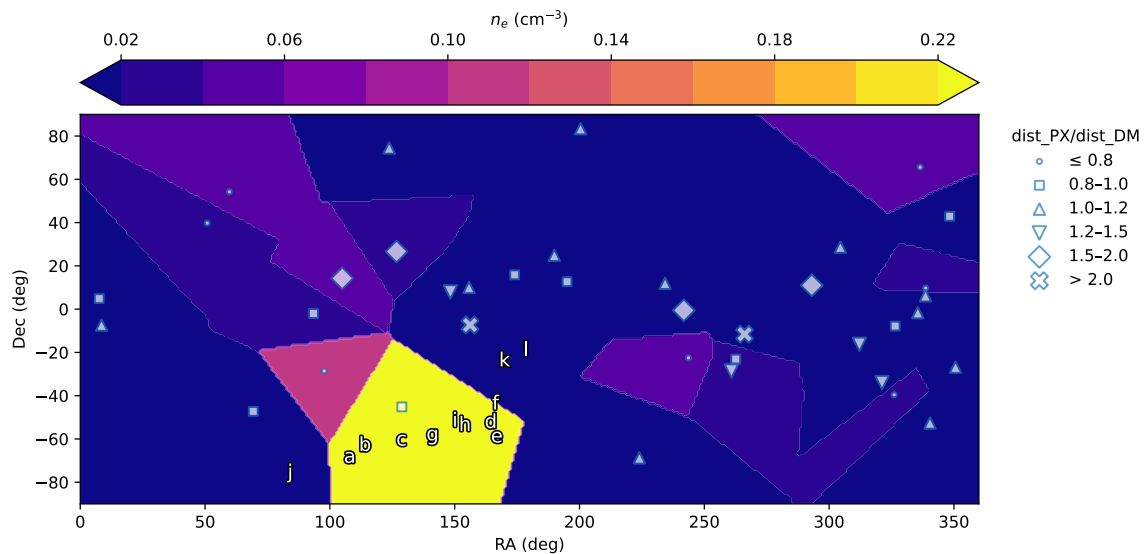
3.2 Parallax-fitted local electron distribution

To create an electron density map for seeking the nearest pulsar, we start by compiling two datasets from the ATNF catalogue, one with pulsars for which a parallax (preferably radio parallax) is reported, and the other with all pulsars within 1 kpc of the Sun.² Then by using the parallax distances of and the DM along the line of sight to these sub-kpc pulsars, we reconstruct the electron number density from Eq. (2.1). Our local n_e map is generated by Gaussian-process regression using a squared-exponential covariance kernel. The kernel’s characteristic angular length scale (i.e. the fitted hyperparameter) is ~ 0.4 rad (approximately 23°), which imposes a natural smoothing of all electron-density features on patches of angular radius $\approx 23^\circ$. In addition, within our 1 kpc sample the mean angular separation between neighboring pulsars is $\approx 17^\circ$, further limiting the map’s intrinsic resolution. Consequently, variations on angular scales below $\approx 15\text{--}20^\circ$ (corresponding to physical sizes $\lesssim 0.3\text{--}0.4$ kpc at 1 kpc) remain unresolved in our reconstruction. We depict contours of this number density in Fig. 1 in equatorial coordinates. (For a representation in Galactocentric coordinates, see Appendix B.)

We have also overlaid the locations of the pulsars used as inputs; for more details on these pulsars, see Appendix A. Note that these sub-kpc pulsars are also part of the 189 pulsars used by YMW [25], except that the fitting model is explicitly suited for larger-than-kpc scales. To illustrate the effect of fluctuations in electron densities, we mark the ratio of their parallax distance to YMW16-based distance using different shapes as explained in the figure legend.

Finally, we also overlay (using white alphabet labels) the locations of pulsars for which there are no parallax estimates, but that which are the closest according to YMW16. We collect these pulsars in the table below the plot, ranking them in increasing order of (the

²In principle catalogues of pulsars discovered by FAST [39–43] and CHIME [44, 45] may also contain specimens within 1 kpc, as derived from the NE2001 and YMW16 models [10]. These may also be included in our analysis but we only include ATNF catalogue pulsars as their properties have been reliably verified.



	PSR	DM (pc cm ⁻³)	δ DM (pc cm ⁻³)	YMW dis (kpc)	Predicted dis (kpc)
a.	J0711–6830	18.4096	0.02	0.106	0.078±0.005
b.	J0736–6304	19.4	-	0.104	0.082±0.005
c.	J0834–60	20	6	0.095	0.084±0.030
d.	J1057–5226	29.69	0.01	0.093	0.125±0.007
e.	J1107–5907	40.75	0.02	0.115	0.172±0.009
f.	J1105–4353	45	-	0.127	0.214±0.012
g.	J0924–5814	57	-	0.107	0.241±0.014
h.	J1016–5345	67	-	0.117	0.284±0.016
i.	J1000–5149	72.8	0.30	0.127	0.307±0.019
j.	J0536–7543	18.6	-	0.127	1.092±0.007
k.	J1120–24	9.81	0.13	0.098	1.560±0.229
l.	J1154–19	10.69	0.05	0.121	1.699±0.235

Figure 1: A new map of the free electron density (blue-yellow colorbar) for the local region, created by fitting with a zeroth-order interpolation of parallax distances to all pulsars with reported parallaxes within 1 kpc. These pulsars are shown as white symbols, and have been classified by the ratio $\text{dist}_{\text{PX}}/\text{dis}_{\text{YMW}}$. Possibly-nearby pulsars without published parallaxes are labeled “a”–“l” in the figure; their YMW-predicted distances and δ DM (where available) are tabulated here alongside our new predicted distances from the revised n_e map. Some pulsar DM measurements reported without error bars are indicated with “-.”

central value of) their distance as per our new map. For each pulsar we propagate both its dispersion-measure uncertainty δ DM and the local Gaussian-process-predicted electron-density uncertainty $\delta n_e(\alpha, \delta)$ via

$$d = \frac{\text{DM}}{n_e(\alpha, \delta)}, \quad \delta d = \sqrt{\left(\frac{\delta \text{DM}}{n_e(\alpha, \delta)}\right)^2 + \left(\frac{\text{DM} \delta n_e(\alpha, \delta)}{[n_e(\alpha, \delta)]^2}\right)^2}, \quad (3.1)$$

where both n_e and δn_e are evaluated at the pulsar’s equatorial coordinates via our regression

model. This yields an uncertainty on each distance estimate that directly reflects the map-inferred electron-density error at that sky location.

Note that these uncertainties do not account for the Lutz-Kelker bias [46] which arises due to the way parallax measurements are distributed and the subsequent statistical treatment of those measurements. The table also provides the DM and YMW16 distance estimates. We note that Vahdat et al. [47] derive an X-ray-absorption-based distance of ~ 860 pc (Section 5.2 of that work). However, that value is not a geometric parallax but is inferred from modelling the soft X-ray hydrogen column density, and thus carries large systematic uncertainties due to inhomogeneous ISM absorption in this direction. By calibrating exclusively to direct parallax measurements (with $\leq 25\%$ uncertainty), our map predicts $d = 78 \pm 5$ pc for PSR J0711–6830. We flag this discrepancy and emphasize that future VLBI parallax observations are necessary to adjudicate between these very different estimates.

Furthermore, wherever applicable, we identify potential optical binary companions to the pulsars which may aid in the precise measurement of pulsar distances, and also provide information on dynamic interactions within such systems. This may be the second best estimate of pulsar distances after radio parallax measurement, if the binary companion can be confirmed through other astrometric data. The identification of an optical or infrared counterpart of a pulsar often relies on finding a star whose position coincides with the pulsar’s location and exhibits characteristics of binarity, *e.g.*, variability and proper motion. To identify binaries in the list of pulsars in the table under Fig. 1, we use the Infrared Science Archive (IRSA) [48], to take a 30 arcsec radial field of view, and cross-reference the resulting objects with the Gaia DR3 database, checking proper motions, locations, and parallaxes; see Table 2 in Appendix A. For pulsars with proper motions reported by ATNF, no promising binary candidates are found. For the rest of the pulsars in our list, only the location and parallax can be used to ascertain the presence of binary counterparts in Gaia DR3. We compare these to the pulsar distances obtained from our revised map. This process identifies potentially four binary companions, which we summarize in Table 3 in Appendix A. We note that the pulsars J1000–5149, J1016–5345, J0924–5814, and J1107–5907 have very low spin-down luminosities ($\dot{E} \lesssim 10^{33}$ erg s $^{-1}$), placing them in a regime where pulsar-wind heating of any companion is effectively negligible. In typical millisecond-pulsar binaries, a white-dwarf companion is rendered optically bright only if \dot{E} exceeds $\sim 10^{34}$ – 10^{35} erg s $^{-1}$; below this threshold its intrinsic cooling emission ($T_{\text{eff}} \lesssim 5000\text{K}$) corresponds to G -band magnitudes $G \gtrsim 20$ – 21 , fainter than the *Gaia*DR3 completeness limit of $G \approx 20.7\text{mag}$ (Gaia Collaboration 2022). Observationally, low- \dot{E} systems rarely exhibit optical counterparts in *Gaia* [49]. Consequently, the absence of *Gaia* detections for these four pulsars is fully consistent with their intrinsic energetics and with the properties expected of millisecond-pulsar white-dwarf companions.

The key outcome of our overall procedure is that, as seen in the table below Fig. 1, our density map predicts a distance of only tens of parsecs to a non-trivial number of pulsars. In contrast, their DM distance per the YMW16 model is around 100–150 pc. As shown in Ref. [10], NSs at $\mathcal{O}(10)$ pc distance are ideal targets for observing late-stage reheating that imparts temperatures of as low as 2500 Kelvin. We will illustrate this further for ELT and TMT in Sec. 4.2. Thus this finding warrants follow-up observations of these pulsars to determine their parallax distance, which would be the most reliable estimate.

4 Prospects for observing dark matter-induced neutron star reheating

As mentioned in the Introduction, NSs may be heated in their late stage by a number of external and internal reheating mechanisms. These include such astrophysical effects [9, 50–65] as rotochemical heating, vortex creep heating, crust-cracking, and magnetic field decay, as well as those induced by a new particle sector [2, 26, 66–68, 68–77, 77–82, 82–110] such as dark matter capture, removal of nucleons from their Fermi seas leading to the so-called nucleon Auger effect, and baryon number-violating neutron decays.

Here we will take dark matter capture as a minimal example, giving rise to kinetic and annihilation heating, and work out the signal expectations at the forthcoming TMT and ELT. We do this to demonstrate a concrete physics case for redrawing the electron density map to the end of seeking the nearest pulsars.

4.1 Review of dark kinetic and annihilation heating

For a detailed description of dark matter-induced heating of NSs, see Ref. [111]. Here we review essential details. Dark matter particles may get captured in astrophysical objects (like NSs) if they scatter and fall into their gravitational potential. The total mass rate of the dark matter going through a NS of mass M and radius R is

$$\begin{aligned} \dot{M}_\chi &= \pi b_{\max}^2 \rho_\chi v_\chi, \\ b_{\max} &= \left(\frac{2GMR}{v_\chi^2} \right)^{1/2} \left(1 - \frac{2GM}{R} \right)^{-1/2} = \gamma R \frac{v_{\text{esc}}}{v_\chi}, \end{aligned} \quad (4.1)$$

where b_{\max} is the maximum impact parameter, $v_{\text{esc}} = \sqrt{2GM/R}$ is the escape speed at the NS surface, and ρ_χ and v_χ are respectively the ambient dark matter density and halo dark matter speed, which we take as 0.42 GeV cm^{-3} and 230 km s^{-1} respectively [112].

The rate of kinetic energy deposition is then

$$\begin{aligned} \dot{E}_k &= \frac{\dot{M}_\chi}{m_\chi} (\gamma - 1) f, \\ f &= \min \left[1, \frac{\sigma_{\chi T}}{\sigma_{\text{crit}}} \right], \end{aligned} \quad (4.2)$$

where f is the fraction of incident dark matter particles that capture, with $\sigma_{\chi T}$ the cross section for scattering with some target (nucleon, lepton, etc.) and σ_{crit} the cross section above which the NS becomes optically thick to the infalling dark matter. Absent Pauli-blocking and multiscatter effects, this is the NS's $\mathcal{O}(10^{-45}) \text{ cm}^{-2}$ geometric cross section.

NSs have internal temperatures of 10^{11} K when formed and cool down through neutrino and photon emission, the latter dominating after $\mathcal{O}(10^5) \text{ yr}$. Until about 10^7 yr an insulating envelope keeps the internal temperature larger than the surface temperature, but beyond this timescale it becomes too thin and the two temperatures become equal, with a value $\leq \mathcal{O}(10^3) \text{ K}$. Under equilibrium between dark kinetic heating and passive cooling,

$$\dot{E}_k = L_{\text{NS}} = 4\pi\sigma_{\text{SB}}R^2T_s^4, \quad (4.3)$$

where σ_{SB} is the Stefan-Boltzmann constant, and T_s is the NS surface blackbody temperature, and for a distant observer, $T_\infty = T_s/\gamma$. Potential NS reheating from astrophysical effects and ISM accretion is in most cases unlikely; see Ref. [2].

If the captured dark matter thermalizes with the NS rapidly enough [91, 113] and self-annihilates efficiently into particles that are trapped in the star, higher heating luminosities are attained. In all, accretion of dark matter that is homogeneously distributed in the halo would give rise to NS surface temperatures of at best around 2500 K near the solar vicinity. Capture of dark matter clumped in overdensities such as microhalos, particularly in models where the dark matter has self-interactions and could thus undergo Bondi accretion, could result in heating-induced NS temperatures of $\mathcal{O}(10^4)$ K [102]. Similar temperatures could be achieved in the presence of long-range interactions between the infalling dark matter and the NS baryons [114]. Motivated by these considerations, we will use reheated NS temperatures of 2500 K, 6000 K, and 10000 K as benchmarks for our treatment of telescope sensitivities.

4.2 Measuring neutron star temperatures with TMT and ELT

The currently operational Near Infrared Camera (NIRCam) on the James Webb Space Telescope (JWST), along with the upcoming Multi-AO Imaging Camera for Deep Observations (MICADO) on the Extremely Large Telescope (ELT) and the future InfraRed Imaging Spectrograph (IRIS) on the Thirty Meter Telescope (TMT) can image in infrared to far-optical wavelengths. These correspond to peak blackbody temperatures of 1300 – 4300 K, making these imaging instruments suitable for detecting NS reheating. As tabulated in Ref. [10], with $10^5 - 10^6$ s of exposure, these instruments could detect $\mathcal{O}(10^3)$ K NSs that are within $\mathcal{O}(10)$ pc and $\mathcal{O}(10^4)$ K NSs within $\mathcal{O}(10^2 - 10^3)$ pc. Here we carry out a similar calculation for the forthcoming ELT-MICADO and TMT-IRIS in order to make our study self-contained.

Assuming the NS to be a black body, the spectral flux density is given by

$$f_\nu = \pi \frac{2h\nu^3}{c^2} \frac{1}{\exp(h\nu/kT_\infty) - 1} \left(\frac{R\gamma}{d} \right)^2, \quad (4.4)$$

often re-expressed in terms of the AB magnitude,

$$m_{\text{AB}} = -2.5 \log_{10} \left(\frac{f_\nu}{3631 \text{ Jy}} \right), \quad (4.5)$$

where R and d are the radius and distance of the NS respectively, and the factor $R\gamma/d$ is the angle subtended by the NS at a distant observer. We have neglected extinction factors along the line of sight, which would introduce uncertainties of at worst 10%, comparable to or smaller than distance uncertainties; see Ref. [10] for a detailed discussion.

Neglecting dithering and read-out pattern effects, the signal-to-noise ratio (SNR) in the background-dominated regime may be approximated as

$$\text{SNR} = \frac{\Phi_{\text{sig}} A_{\text{SNR}} t_{\text{exp}}}{\sqrt{(\Phi_{\text{bg}} A_{\text{SNR}} + \Gamma_{\text{noise}}) t_{\text{exp}}}}, \quad (4.6)$$

where Φ_{sig} and Φ_{bg} are signal and background fluxes, A_{SNR} is the SNR reference area in the detector, and Γ_{noise} is the non-sky noise rate. Thus we expect $t_{\text{exp}} \propto (\text{SNR})^2$, and using this in Eq. (4.4), we have the scaling $t_{\text{exp}} \propto d^4$. In the left panel of Fig. 2 we plot the AB magnitudes as a function of neutron-star distance for surface temperatures of 2500 K (solid lines) and 10000 K (dashed lines), over a range of mass–radius configurations. As expected from Eqs. (4.4) and (4.5), $m_{\text{AB}} \propto \log d$, and more massive or larger stars appear brighter. In the right panel we plot the signal-to-noise ratio versus total exposure time for neutron stars at fiducial distances of 50 pc and 100 pc. For ELT–MICADO we display only

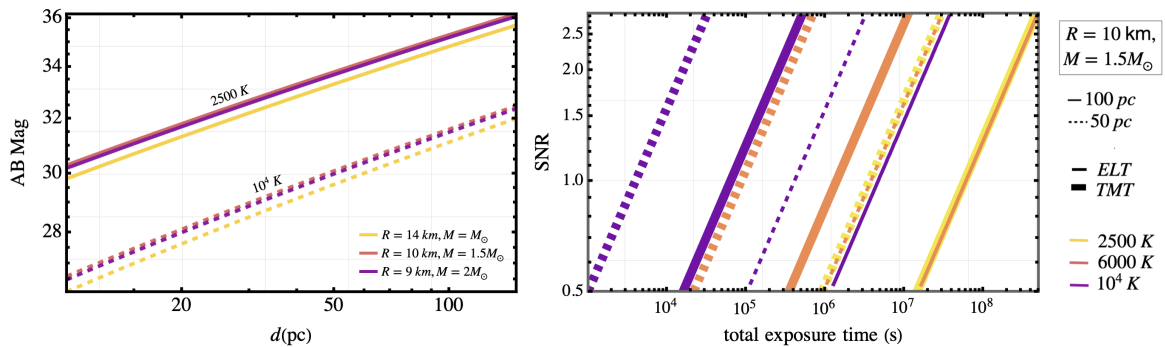


Figure 2: **Left:** AB magnitude derived for neutron stars heated maximally by kinetic and annihilation heating of dark matter to reach a temperature of 2500 K (solid lines) and 10⁴ K (dashed lines) for different radius and mass profiles. **Right:** Predicted signal-to-noise ratio (SNR) as a function of total exposure time for neutron stars at 50 (dashed lines) and 100 (solid lines) pc, computed with the MICADO ETC for the ELT and the IRIS ETC for the TMT. For ELT–MICADO we choose the B band for $T_{\text{eff}} = 6000$ K and the U band for $T_{\text{eff}} = 10^4$ K, so as to sample the blackbody peak in each case. For TMT–IRIS, we use the Y-band filter—although it does not fall at the peak of the 6000 K or 10⁴ K spectra, its wide bandwidth and high throughput still yield strong photon counts and competitive sensitivities. All calculations assume a canonical neutron-star radius of $R = 10$ km and mass $M = 1.5 M_{\odot}$. Note that exposures much longer than a few 10⁷ s (\sim yr) may be unrealistic, although this exposure time is comparable to prior ultra deep field observations [115].

the $T = 6000$ K (B-band) and $T = 10^4$ K (U-band) curves, since at J-band the required exposure times exceed 10⁸ s—well beyond practical limits. For TMT–IRIS we show all three temperature benchmarks ($T = 2500$ K, 6000 K, and 10⁴ K) using the Y-band filter. Although Y-band does not coincide exactly with the spectral peaks of the higher-temperature cases, its broad passband and high throughput still yield robust SNR estimates. This choice provides a conservative, proof-of-concept sensitivity in the absence of B or U filters in the current TMT–IRIS ETC. For the ELT, we set the source geometry to be a point source with the source spectral type corresponding to the temperature profile being considered, with a S/N reference area of 1×1 pixels at the Paranal observation site at 2635 m, with a telescope diameter of 39 m, and we use the default background model. Furthermore, we use typical values for air-mass of 1.50, pixel scale of 50 mas/pixel and seeing limited (FWHM = 0".8) adaptive optics mode. Similarly for TMT, we set the source geometry to be a point source, at a zenith angle of 0 in good weather conditions, under the Imager mode configuration. In this figure we see the scaling $\text{SNR} \propto \sqrt{t_{\text{exp}}} \propto d^2$. We also find the results consistent with Ref. [10].

5 Conclusion

The aim of this study is to initiate a robust search for neutron stars nearest to Earth. A close enough NS would be a target for observing, among other things, novel late-time reheating mechanisms including from the capture of dark matter. To this end, we have attempted to refine the electron density map in the solar vicinity, in turn improving the accuracy of dispersion measure-driven distance estimates for pulsars.

In particular, using parallax measurements of pulsar distances (which are unrelated to DM-based distance estimates) we constructed a simplified electron density map. This revised map allowed us to pinpoint promising nearby pulsar candidates that are ideal for follow-up parallax observations, as summarized in the table in Figure 1. We also investigated the possibility of finding binary stellar counterparts for these pulsars, summarized in Table 2.

We believe our map may offer a more accurate depiction of pulsar locations within the 1 kpc vicinity than the earlier NE2001 and YMW16 models, which had focused on large-scale galactic DMs, and included a template fit to assumed locations of electron over-densities and under-densities. In contrast, by only concentrating on the local kpc, we provide a new estimate of the free electron density. Looking forward, more accurate estimates of distances to nearby NSs such as those undertaken in this study are an essential step to begin fathoming some longstanding puzzles of fundamental physics.

Acknowledgments

We thank M. A. Krishnakumar, Joseph Lazio, and Avinash Kumar Paladi for helpful discussions and correspondence. This work was supported by the Arthur B. McDonald Canadian Astroparticle Physics Research Institute, the Natural Sciences and Engineering Research Council of Canada (NSERC), and the Canada Foundation for Innovation. Research at Perimeter Institute is supported by the Government of Canada through the Department of Innovation, Science, and Economic Development, and by the Province of Ontario. This research has made use of the NASA/IPAC Infrared Science Archive (IRSA), which is funded by the National Aeronautics and Space Administration and operated by the California Institute of Technology, the NASA/IPAC Extragalactic Database (NED), which is operated by the Jet Propulsion Laboratory, California Institute of Technology, under contract with the National Aeronautics and Space Administration. LS is supported by the National SKA Program of China (2020SKA0120300) and the Max Planck Partner Group Program funded by the Max Planck Society.

Appendices

A Pulsar properties

In this section we collect details of pulsars used in this work. In Table 1 are the pulsars used to construct our electron density map in Fig. 1 and Fig. 3. In Table 2 are the pulsars for which we have estimated DM-based distances using our revised map. These are the same pulsars as those tabulated below Fig. 1, but now we provide further details such as their proper motion. This information is used to identify potential binary companions, listed in Table 3.

Table 1: Pulsars used to construct our local electron density map in Fig. 1 (and Fig. 3), along with their reported parallax, equatorial co-ordinate positions, dispersion measure, parallax distance and YMW-based distance.

PSR	PX (mas)	RAJD (deg)	DECJD (deg)	DM ($\text{cm}^{-3} \text{ pc}$)	dis _{PX} (kpc)	dis _{YMW} (kpc)
J0030+0451	2.910 ± 0.180	7.61	4.86	4.33294 ± 0.00011	0.344	0.345
J0034-0721	0.930 ± 0.080	8.54	-7.36	10.92200 ± 0.00600	1.075	0.996
J0323+3944	1.051 ± 0.040	50.86	39.75	26.18975 ± 0.00093	0.951	1.197
J0358+5413	0.910 ± 0.160	59.72	54.22	57.14200 ± 0.00030	1.099	1.594
J0437-4715	6.430 ± 0.040	69.32	-47.25	2.64476 ± 0.00007	0.156	0.156
J0613-0200	1.010 ± 0.090	93.43	-2.01	38.77500 ± 0.00050	0.990	1.024
J0630-2834	3.009 ± 0.409	97.71	-28.58	34.42500 ± 0.00100	0.332	2.069
J0659+1414	3.470 ± 0.360	1 04.95	14.24	13.94000 ± 0.09000	0.288	0.159
J0737-3039A/B	0.870 ± 0.140	114.46	-30.66	48.91600 ± 0.00200	1.149	1.105
J0814+7429	2.310 ± 0.040	123.75	74.48	5.75066 ± 0.00048	0.433	0.368
J0826+2637	2.010 ± 0.013	126.71	26.62	19.47633 ± 0.00018	0.498	0.314
J0835-4510	3.500 ± 0.200	128.84	-45.18	67.77100 ± 0.00900	0.286	0.328
J0953+0755	3.820 ± 0.070	148.29	7.93	2.96927 ± 0.00008	0.262	0.187
J1022+1001	1.160 ± 0.080	155.74	10.03	10.25500 ± 0.00080	0.862	0.834
J1024-0719	0.970 ± 0.130	156.16	-7.32	6.48640 ± 0.00020	1.031	0.382
J1136+1551	2.687 ± 0.018	174.01	15.85	4.84066 ± 0.00034	0.372	0.414
J1239+2453	1.160 ± 0.080	189.92	24.90	9.25159 ± 0.00053	0.862	0.827
J1300+1240	1.410 ± 0.080	195.01	12.68	10.16550 ± 0.00003	0.709	0.877
J1321+8323	0.968 ± 0.140	200.44	83.39	13.31624 ± 0.00076	1.033	0.977
J1456-6843	2.200 ± 0.300	224.00	-68.73	8.61300 ± 0.00400	0.455	0.436
J1537+1155	1.070 ± 0.090	234.29	11.93	11.61944 ± 0.00002	0.935	0.877
J1607-0032	0.934 ± 0.047	241.80	-0.54	10.68230 ± 0.00010	1.071	0.680
J1614-2230	1.300 ± 0.200	243.65	-22.51	34.48500 ± 0.00030	0.769	1.394
J1723-2837	1.077 ± 0.054	260.85	-28.63	19.68800 ± 0.01300	0.929	0.720
J1730-2304	2.300 ± 0.200	262.59	-23.08	9.62570 ± 0.00050	0.435	0.512
J1744-1134	2.610 ± 0.090	266.12	-11.58	3.13849 ± 0.00012	0.383	0.148
J1932+1059	2.770 ± 0.070	293.06	10.99	3.18321 ± 0.00016	0.361	0.229
J2018+2839	1.030 ± 0.100	304.52	28.67	14.19770 ± 0.00060	0.971	0.959
J2048-1616	1.050 ± 0.030	312.15	-16.28	11.45600 ± 0.00500	0.952	0.775
J2124-3358	2.300 ± 0.200	321.18	-33.98	4.59540 ± 0.00030	0.435	0.360
J2144-3933	6.051 ± 0.560	326.05	-39.57	3.35000 ± 0.01000	0.165	0.289

Continued on next page

Table 1 – continued from previous page

PSR	PX (mas)	RAJD (deg)	DECJD (deg)	DM (cm^{-3}pc)	dis _{PX} (kpc)	dis _{YMW} (kpc)
J2145-0750	1.600 ± 0.300	326.46	-7.84	9.00080 ± 0.00130	0.625	0.693
J2222-0137	3.723 ± 0.014	335.52	-1.62	3.28260 ± 0.00020	0.269	0.267
J2225+6535	1.203 ± 0.204	336.47	65.59	36.44362 ± 0.00051	0.831	1.881
J2234+0611	1.050 ± 0.040	338.60	6.19	10.76700 ± 0.00020	0.952	0.854
J2234+0944	1.300 ± 0.400	338.70	9.74	17.83230 ± 0.00020	0.769	1.587
J2241-5236	0.960 ± 0.040	340.43	-52.61	11.41126 ± 0.00003	1.042	0.963
J2313+4253	0.930 ± 0.070	348.29	42.89	17.27693 ± 0.00033	1.075	1.108
J2322-2650	1.300 ± 0.200	350.64	-26.85	6.14906 ± 0.00013	0.769	0.760

	PSR	RA (deg)	DEC (deg)	Pred. dist. (kpc)	PM RA (mas/yr)	PM DEC (mas/yr)	PM tot (mas/yr)	Potential binary
a.	J0711-6830	107.97	-68.51	0.078 ± 0.005	-15.56 ± 9	14.18 ± 9	21.05 ± 9	
b.	J0736-6304	114.08	-63.07	0.082 ± 0.005	—	—	—	
c.	J0834-60	128.71	-60.58	0.084 ± 0.030	—	—	—	
d.	J1057-5226	164.49	-52.44	0.125 ± 0.007	47.5 ± 7	-8.7 ± 7	48.3 ± 7	
e.	J1107-5907	166.89	-59.12	0.172 ± 0.009	—	—	—	Gaia DR3 5338633770476031360
f.	J1105-4353	166.35	-43.88	0.189 ± 0.011	—	—	—	
g.	J0924-5814	141.13	-58.23	0.241 ± 0.014	—	—	—	Gaia DR3 5306447697839727360
h.	J1016-5345	154.13	-53.75	0.284 ± 0.016	—	—	—	Gaia DR3 5356512791576521984
i.	J1000-5149	150.12	-51.83	0.307 ± 0.019	—	—	—	Gaia DR3 5405166971370873216
j.	J0536-7543	84.13	-75.73	1.092 ± 0.007	3 ± 40	65 ± 8	65 ± 9	
k.	J1120-24	170.00	-24.00	0.824 ± 0.068	—	—	—	
l.	J1154-19	178.50	-19.00	0.822 ± 0.009	—	—	—	

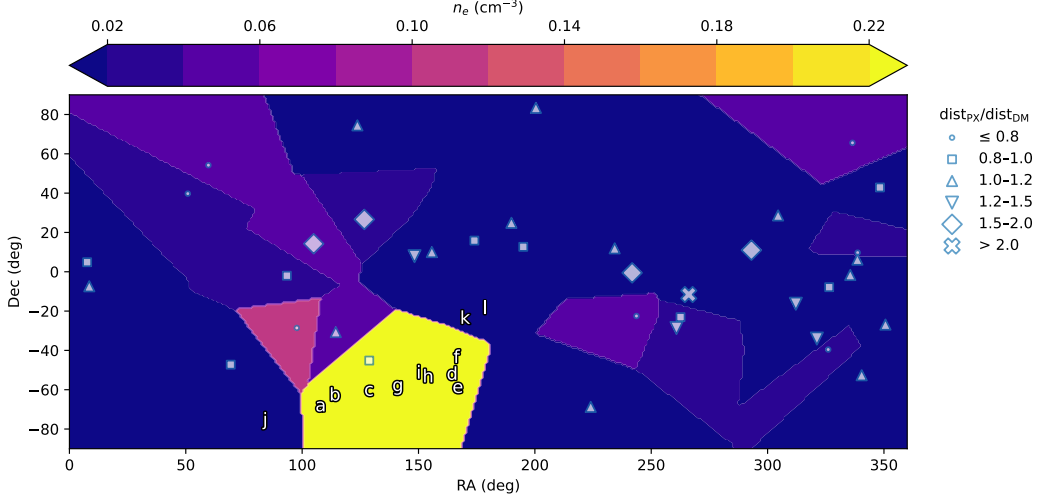
Table 2: Pulsars (a–l) referenced in Figs. 1 & 3, with their predicted distances from our n_e map(Fig. 3, proper motions, and any Gaia DR3 companion.

Potential binary	RA (deg)	DEC (deg)	PM RA (mas/yr)	PM DEC (mas/yr)	PM tot (mas/yr)	PX (mas)	dist _{PX} (kpc)	Assoc. PSR	Pred. dist. (kpc)
Gaia DR3 5338633770476031360	166.91	-59.12	-4.25 ± 1.24	2.35 ± 1.10	4.86	3.13 ± 1.46	0.319	J1107-5907	0.172 ± 0.009
Gaia DR3 5306447697839727360	141.14	-58.23	-3.56 ± 0.92	3.39 ± 1.21	4.91	1.54 ± 1.03	0.649	J0924-5814	0.241 ± 0.014
Gaia DR3 5356512791576521984	154.14	-53.75	-5.03 ± 0.94	2.17 ± 0.93	5.48	1.72 ± 0.73	0.581	J1016-5345	0.284 ± 0.016
Gaia DR3 5405166971370873216	150.12	-51.83	-5.09 ± 1.08	4.80 ± 0.95	7.00	1.73 ± 0.81	0.578	J1000-5149	0.307 ± 0.019

Table 3: Gaia DR3 counterparts to the pulsars in Table 2, with their parallaxes and parallax distances, compared to the predicted distances from our n_e map(Fig. 3.)

B Modified electron density map in galactocentric representation

In this section, we re-create Fig. 1, with the region of interest extended to 1.1 kpc.



	PSR	DM (pc cm^{-3})	δDM (pc cm^{-3})	YMW dis (kpc)	Predicted dis (kpc)
a.	J0711–6830	18.4096	0.02	0.106	0.078 ± 0.005
b.	J0736–6304	19.4	-	0.104	0.082 ± 0.005
c.	J0834–60	20	6	0.095	0.084 ± 0.030
d.	J1057–5226	29.69	0.01	0.093	0.125 ± 0.007
e.	J1107–5907	40.75	0.02	0.115	0.172 ± 0.009
f.	J1105–4353	45	-	0.127	0.189 ± 0.011
g.	J0924–5814	57	-	0.107	0.241 ± 0.014
h.	J1016–5345	67	-	0.117	0.284 ± 0.016
i.	J1000–5149	72.8	0.30	0.127	0.307 ± 0.019
j.	J0536–7543	18.6	-	0.127	1.092 ± 0.007
k.	J1120–24	9.81	0.13	0.098	0.824 ± 0.068
l.	J1154–19	10.69	0.05	0.121	0.822 ± 0.009

Figure 3: Map of the free electron density (blue to yellow color bar) for the extended region of 1.1 kpc, created by fitting with a zeroth-order interpolation of parallax distances to all pulsars with reported parallax measurements that are within 1.1 kpc of Earth. These pulsars are displayed as white symbols, and have been classified according to the ratio of their distance estimates from parallax (dis_{PX}) and from the YMW16 model (dis_{YMW}). Possibly nearby pulsars that do not yet have parallax measurements made on them are tabulated and labeled “a”–“l” in the figure. Their YMW16 predicted distances and δDM (where available) are listed in the table alongside new predicted distances derived from our revised electron density map. Discrepancies with Table 1 are seen to be conspicuous near the 1 kpc scale.

Next, we re-display pulsar positions from Fig. 3 in galactocentric right-handed rectangular coordinates in Fig. 4. Here the X axis is directed toward the Galactic Center, the Y axis spans longitude and the Z axis spans latitude.

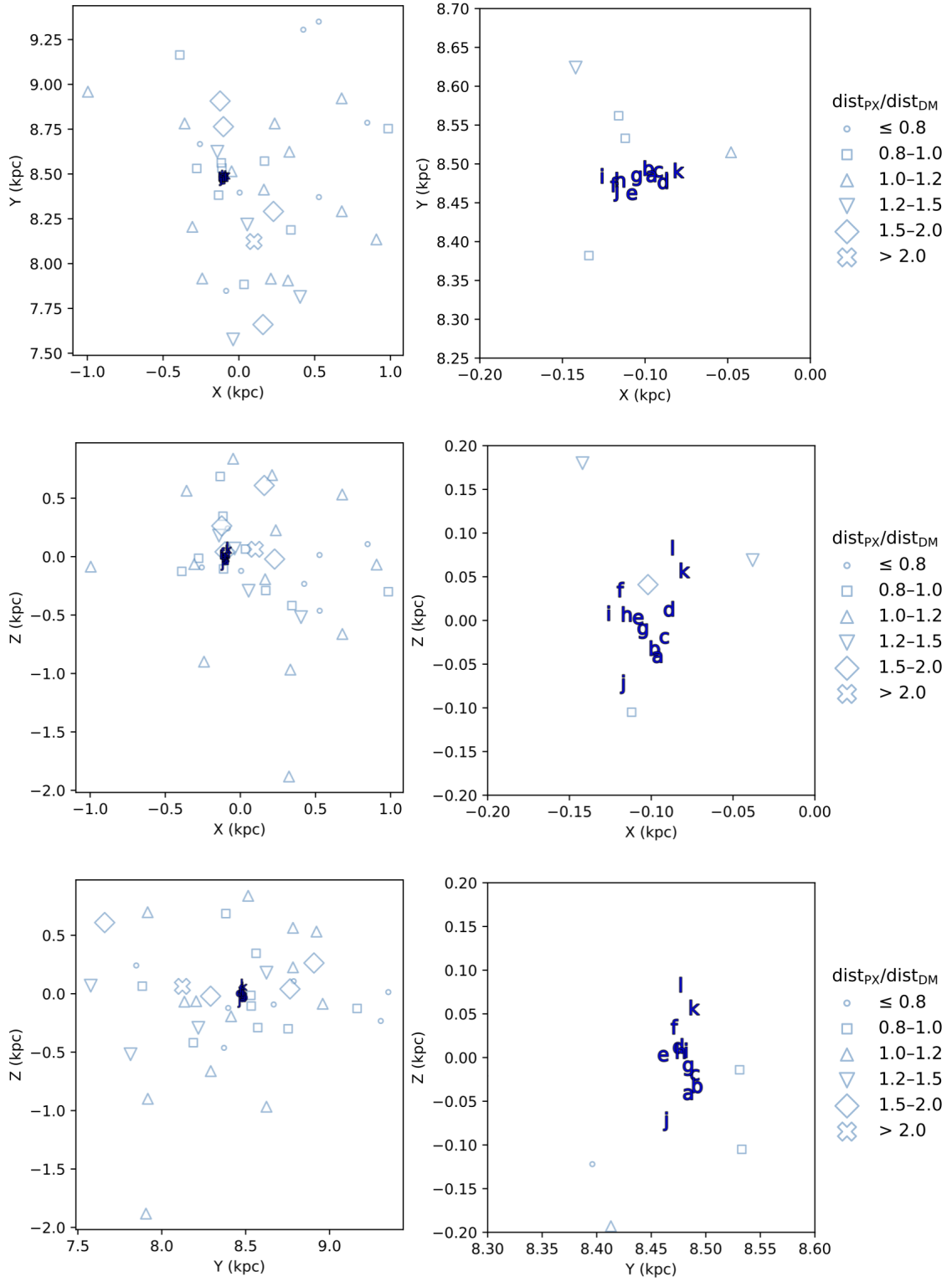


Figure 4: Projected pulsar positions in Galactocentric rectangular coordinates. The left column shows the side-view (X–Y), top-view (X–Z) and front-view (Y–Z) slices. Pulsars with reported parallax distances are classified according to the ratio of their distance estimates from parallax and from the YMW16 model (shown by white symbols), $\text{dist}_{\text{PX}}/\text{dist}_{\text{DM}}$, and nearby candidates without measured parallaxes are marked by red labels “a”–“l.” The right-hand panels are zoomed in on the same regions to highlight those labeled sources.

References

- [1] J. Nättilä and J. J. E. Kajava, *Fundamental physics with neutron stars*, [arXiv:2211.15721](#).
- [2] J. Bramante and N. Raj, *Dark matter in compact stars*, *Phys. Rept.* **1052** (2024) 1–48, [[arXiv:2307.14435](#)].
- [3] L. Shao and K. Yagi, *Neutron stars as extreme laboratories for gravity tests*, *Sci. Bull.* **67** (2022) 1946–1949, [[arXiv:2209.03351](#)].
- [4] J. M. Lattimer and M. Prakash, *Neutron star structure and the equation of state*, *Astrophys. J.* **550** (2001) 426, [[astro-ph/0002232](#)].
- [5] N. Tetzlaff, R. Neuhauser, M. M. Hohle, and G. Maciejewski, *Identifying birth places of young isolated neutron stars*, *MNRAS* **402** (Mar., 2010) 2369–2387, [[arXiv:0911.4441](#)].
- [6] D. G. Yakovlev and C. J. Pethick, *Neutron star cooling*, *Ann. Rev. Astron. Astrophys.* **42** (2004) 169–210, [[astro-ph/0402143](#)].
- [7] D. Page, J. M. Lattimer, M. Prakash, and A. W. Steiner, *Minimal cooling of neutron stars: A New paradigm*, *Astrophys. J. Suppl.* **155** (2004) 623–650, [[astro-ph/0403657](#)].
- [8] A. Y. Potekhin, D. A. Zyuzin, D. G. Yakovlev, M. V. Beznogov, and Y. A. Shibano, *Thermal luminosities of cooling neutron stars*, *Mon. Not. Roy. Astron. Soc.* **496** (2020), no. 4 5052–5071, [[arXiv:2006.15004](#)].
- [9] D. Gonzalez and A. Reisenegger, *Internal heating of old neutron stars: contrasting different mechanisms*, *AAP* **522** (Nov., 2010) A16, [[arXiv:1005.5699](#)].
- [10] N. Raj, P. Shivanna, and G. N. Rachh, *Exploring reheated sub-40000 Kelvin neutron stars with JWST, ELT, and TMT*, *Phys. Rev. D* **109** (2024), no. 12 123040, [[arXiv:2403.07496](#)].
- [11] D. R. Lorimer, *Radio pulsar populations*, *Astrophys. Space Sci. Proc.* (2011) 21–36, [[arXiv:1008.1928](#)].
- [12] F. M. Walter, T. Eisenbeiss, J. M. Lattimer, B. Kim, V. Hambaryan, and R. Neuhaeuser, *Revisiting the Parallax of the Isolated Neutron Star RX J185635-3754 Using HST/ACS Imaging*, *Astrophys. J.* **724** (2010) 669–677, [[arXiv:1008.1709](#)].
- [13] L.-L. Zheng, M. Sun, W.-M. Gu, T. Yi, Z.-X. Zhang, P. Wang, J. Wang, J. Wu, S. Wang, J. Zhang, C.-Q. Li, J.-R. Shi, Y. Shao, X.-D. Li, J.-B. Fu, F. Yang, Z. Bai, Y. Bai, H. Zhang, and J. Liu, *The Nearest Neutron Star Candidate in a Binary Revealed by Optical Time-domain Surveys*, *arXiv e-prints* (Oct., 2022) arXiv:2210.04685, [[arXiv:2210.04685](#)].
- [14] O. Blaes and P. Madau, *Can We Observe Accreting, Isolated Neutron Stars?*, *Astrophysical Journal* **403** (Feb., 1993) 690.
- [15] N. Sartore, E. Ripamonti, A. Treves, and R. Turolla, *Galactic neutron stars*, *Astronomy and Astrophysics* **510** (Feb, 2010) A23.
- [16] R. N. Manchester, G. B. Hobbs, A. Teoh, and M. Hobbs, *The australia telescope national facility pulsar catalogue*, *The Astronomical Journal* **129** (apr, 2005) 1993–2006.
- [17] R. S. Lynch, J. K. Swiggum, V. I. Kondratiev, D. L. Kaplan, K. Stovall, E. Fonseca, M. S. E. Roberts, L. Levin, M. E. DeCesar, B. Cui, S. B. Cenko, P. Gatkine, A. M. Archibald, S. Banaszak, C. M. Biwer, J. Boyles, P. Chawla, L. P. Dartez, D. Day, A. J. Ford, J. Flanigan, J. W. T. Hessels, J. Hinojosa, F. A. Jenet, C. Karako-Argaman, V. M. Kaspi, S. Leake, G. Lunsford, J. G. Martinez, A. Mata, M. A. McLaughlin, H. A. Noori, S. M. Ransom, M. D. Rohr, X. Siemens, R. Spiewak, I. H. Stairs, J. van Leeuwen, A. N. Walker, and B. L. Wells, *The Green Bank North Celestial Cap Pulsar Survey. III. 45 New Pulsar Timing Solutions*, *Astrophysical Journal* **859** (June, 2018) 93, [[arXiv:1805.04951](#)].
- [18] K. Stovall, R. S. Lynch, S. M. Ransom, A. M. Archibald, S. Banaszak, C. M. Biwer, J. Boyles, L. P. Dartez, D. Day, A. J. Ford, J. Flanigan, A. Garcia, J. W. T. Hessels, J. Hinojosa, F. A.

- Jenet, D. L. Kaplan, C. Karako-Argaman, V. M. Kaspi, V. I. Kondratiev, S. Leake, D. R. Lorimer, G. Lunsford, J. G. Martinez, A. Mata, M. A. McLaughlin, M. S. E. Roberts, M. D. Rohr, X. Siemens, I. H. Stairs, J. van Leeuwen, A. N. Walker, and B. L. Wells, *The Green Bank Northern Celestial Cap Pulsar Survey. I. Survey Description, Data Analysis, and Initial Results*, *APJ* **791** (Aug., 2014) 67, [[arXiv:1406.5214](#)].
- [19] G. Y. Agazie, M. G. Mingyar, M. A. McLaughlin, J. K. Swiggum, D. L. Kaplan, H. Blumer, P. Chawla, M. DeCesar, P. B. Demorest, W. Fiore, E. Fonseca, J. D. Gelfand, V. M. Kaspi, V. I. Kondratiev, M. LaRose, J. van Leeuwen, L. Levin, E. F. Lewis, R. S. Lynch, A. E. McEwen, H. Al Noori, E. Parent, S. M. Ransom, M. S. E. Roberts, A. Schmiiedekamp, C. Schmiiedekamp, X. Siemens, R. Spiewak, I. H. Stairs, and M. Surnis, *The Green Bank Northern Celestial Cap Pulsar Survey. VI. Discovery and Timing of PSR J1759+5036: A Double Neutron Star Binary Pulsar*, *Astrophysical Journal* **922** (Nov., 2021) 35, [[arXiv:2102.10214](#)].
- [20] A. E. McEwen, R. Spiewak, J. K. Swiggum, D. L. Kaplan, W. Fiore, G. Y. Agazie, H. Blumer, P. Chawla, M. DeCesar, V. M. Kaspi, V. I. Kondratiev, M. LaRose, L. Levin, R. S. Lynch, M. McLaughlin, M. Mingyar, H. A. Noori, S. M. Ransom, M. S. E. Roberts, A. Schmiiedekamp, C. Schmiiedekamp, X. Siemens, I. Stairs, K. Stovall, M. Surnis, and J. van Leeuwen, *The Green Bank North Celestial Cap Pulsar Survey. V. Pulsar Census and Survey Sensitivity*, *Astrophysical Journal* **892** (Apr., 2020) 76, [[arXiv:1909.11109](#)].
- [21] R. J. Aloisi, A. Cruz, L. Daniels, N. Meyers, R. Roekle, A. Schuett, J. K. Swiggum, M. E. DeCesar, D. L. Kaplan, R. S. Lynch, K. Stovall, L. Levin, A. M. Archibald, S. Banaszak, C. M. Biwer, J. Boyles, P. Chawla, L. P. Dartez, B. Cui, D. F. Day, A. J. Ford, J. Flanigan, E. Fonseca, J. W. T. Hessels, J. Hinojosa, C. Karako-Argaman, V. M. Kaspi, V. I. Kondratiev, S. Leake, G. Lunsford, J. G. Martinez, A. Mata, M. A. McLaughlin, H. A. Noori, S. M. Ransom, M. S. E. Roberts, M. D. Rohr, X. Siemens, R. Spiewak, I. H. Stairs, J. van Leeuwen, A. N. Walker, and B. L. Wells, *The Green Bank North Celestial Cap Pulsar Survey. IV. Four New Timing Solutions*, *Astrophysical Journal* **875** (Apr., 2019) 19, [[arXiv:1903.03543](#)].
- [22] A. M. Kawash, M. A. McLaughlin, D. L. Kaplan, M. E. DeCesar, L. Levin, D. R. Lorimer, R. S. Lynch, K. Stovall, J. K. Swiggum, E. Fonseca, A. M. Archibald, S. Banaszak, C. M. Biwer, J. Boyles, B. Cui, L. P. Dartez, D. Day, S. Ernst, A. J. Ford, J. Flanigan, S. A. Heatherly, J. W. T. Hessels, J. Hinojosa, F. A. Jenet, C. Karako-Argaman, V. M. Kaspi, V. I. Kondratiev, S. Leake, G. Lunsford, J. G. Martinez, A. Mata, T. D. Matheny, A. E. McEwen, M. G. Mingyar, A. L. Orsini, S. M. Ransom, M. S. E. Roberts, M. D. Rohr, X. Siemens, R. Spiewak, I. H. Stairs, J. van Leeuwen, A. N. Walker, and B. L. Wells, *The Green Bank Northern Celestial Cap Pulsar Survey. II. The Discovery and Timing of 10 Pulsars*, *Astrophysical Journal* **857** (Apr., 2018) 131, [[arXiv:1803.03587](#)].
- [23] D. R. Lorimer, N. D’Amico, A. G. Lyne, J. H. Seiradakis, A. Athanasopoulos, F. Camilo, A. Jessner, M. Kramer, R. Wielebinski, and K. M. Xilouris, *The European Pulsar Network Pulse Profile Database*, in *Joint European and National Astronomical Meeting* (J. D. Hadjidemetriou and J. H. Seiradakis, eds.), p. 236, Jan., 1997.
- [24] J. M. Cordes and T. J. W. Lazio, *NE2001. 1. A New model for the galactic distribution of free electrons and its fluctuations*, [astro-ph/0207156](#).
- [25] J. M. Yao, R. N. Manchester, and N. Wang, *A NEW ELECTRON-DENSITY MODEL FOR ESTIMATION OF PULSAR AND FRB DISTANCES*, *The Astrophysical Journal* **835** (jan, 2017) 29.
- [26] M. Baryakhtar, J. Bramante, S. W. Li, T. Linden, and N. Raj, *Dark Kinetic Heating of Neutron Stars and An Infrared Window On WIMPs, SIMPs, and Pure Higgsinos*, *Phys. Rev. Lett.* **119** (2017), no. 13 131801, [[arXiv:1704.01577](#)].
- [27] J. Bramante, B. J. Kavanagh, and N. Raj, *Scattering Searches for Dark Matter in Subhalos:*

- Neutron Stars, Cosmic Rays, and Old Rocks*, *Phys. Rev. Lett.* **128** (2022), no. 23 231801, [[arXiv:2109.04582](https://arxiv.org/abs/2109.04582)].
- [28] S. Guillot, G. G. Pavlov, C. Reyes, A. Reisenegger, L. Rodriguez, B. Rangelov, and O. Kargaltsev, *Hubble Space Telescope Nondetection of PSR J2144–3933: The Coldest Known Neutron Star*, *Astrophys. J.* **874** (2019), no. 2 175, [[arXiv:1901.07998](https://arxiv.org/abs/1901.07998)].
- [29] M. A. de Avillez, G. J. Anela, A. Asgekar, D. Breitschwerdt, and D. H. F. M. Schnitzeler, *Electrons in the supernova-driven interstellar medium. Results from self-consistent time-dependent ionic and hydrodynamic evolution of the interstellar plasma*, *AAP* **644** (Dec., 2020) A156.
- [30] S. R. Kulkarni, *Dispersion measure: Confusion, Constants & Clarity*, [arXiv:2007.02886](https://arxiv.org/abs/2007.02886).
- [31] J. H. Taylor and J. M. Cordes, *Pulsar Distances and the Galactic Distribution of Free Electrons*, *APJ* **411** (July, 1993) 674.
- [32] N. D. R. Bhat, Y. Gupta, and A. P. Rao, *Pulsar Scintillation and the Local Bubble*, *APJ* **500** (June, 1998) 262–279, [[astro-ph/9802203](https://arxiv.org/abs/astro-ph/9802203)].
- [33] **NANOGrav** Collaboration, A. M. Matthews et al., *The NANOGrav Nine-year Data Set: Astrometric Measurements of 37 Millisecond Pulsars*, *Astrophys. J.* **818** (2016), no. 1 92, [[arXiv:1509.08982](https://arxiv.org/abs/1509.08982)].
- [34] D. J. Reardon et al., *Timing analysis for 20 millisecond pulsars in the Parkes Pulsar Timing Array*, *Mon. Not. Roy. Astron. Soc.* **455** (2016), no. 2 1751–1769, [[arXiv:1510.04434](https://arxiv.org/abs/1510.04434)].
- [35] A. T. Deller et al., *Microarcsecond VLBI Pulsar Astrometry with PSR π II. Parallax Distances for 57 Pulsars*, *Astrophys. J.* **875** (2019), no. 2 100, [[arXiv:1808.09046](https://arxiv.org/abs/1808.09046)].
- [36] A. Deller, *Pulsar distance measurements with VLBI*, in *40th COSPAR Scientific Assembly*, vol. 40, pp. E1.15–5–14, Jan., 2014.
- [37] B. Posselt, G. Spence, and G. G. Pavlov, *A Chandra Search for the Pulsar Wind Nebula Around psr B1055–52*, *Astrophys. J.* **811** (2015), no. 2 96, [[arXiv:1507.07924](https://arxiv.org/abs/1507.07924)].
- [38] R. P. Mignani, G. G. Pavlov, and O. Kargaltsev, *Optical-Ultraviolet Spectrum and Proper Motion of the Middle-aged Pulsar B1055-52*, *Astrophysical Journal* **720** (Sept., 2010) 1635–1643, [[arXiv:1007.2940](https://arxiv.org/abs/1007.2940)].
- [39] **FAST** Collaboration, “FAST-CRAFTS pulsar catalogue.” http://groups.bao.ac.cn/ism/CRAFTS/202203/t20220310_683697.html.
- [40] **FAST** Collaboration, “FAST-GPPS pulsar catalogue.” <http://zmtt.bao.ac.cn/GPPS/GPPSnewPSR.html>.
- [41] J. L. Han et al., *The FAST Galactic Plane Pulsar Snapshot survey: I. Project design and pulsar discoveries*, *Res. Astron. Astrophys.* **21** (2021) 107, [[arXiv:2105.08460](https://arxiv.org/abs/2105.08460)].
- [42] D. J. Zhou et al., *The FAST Galactic Plane Pulsar Snapshot Survey. II. Discovery of 76 Galactic Rotating Radio Transients and the Enigma of RRATs*, *Res. Astron. Astrophys.* **23** (2023), no. 10 104001, [[arXiv:2303.17279](https://arxiv.org/abs/2303.17279)].
- [43] W. Q. Su et al., *The FAST Galactic Plane Pulsar Snapshot Survey – III. Timing results of 30 newly discovered pulsars*, *Mon. Not. Roy. Astron. Soc.* **526** (2023), no. 2 2645–2656, [[arXiv:2305.16754](https://arxiv.org/abs/2305.16754)].
- [44] **CHIME** Collaboration, “CHIME pulsar catalogue.” <https://www.chime-frb.ca/galactic>.
- [45] F. A. Dong et al., *The second set of pulsar discoveries by CHIME/FRB/Pulsar: 14 rotating radio transients and 7 pulsars*, *Mon. Not. Roy. Astron. Soc.* **524** (2023), no. 4 5132–5147, [[arXiv:2210.09172](https://arxiv.org/abs/2210.09172)].
- [46] T. E. Lutz and D. H. Kelker, *On the Use of Trigonometric Parallaxes for the Calibration of Luminosity Systems: Theory*, *Publications of the ASP* **85** (Oct., 1973) 573.

- [47] A. Vahdat, B. Posselt, A. Santangelo, and G. G. Pavlov, *Toward an X-ray inventory of nearby neutron stars*, *AAP* **658** (Feb., 2022) A95, [[arXiv:2111.04791](#)].
- [48] **FAST** Collaboration, “FAST-CRAFTS pulsar catalogue.” <https://irsa.ipac.caltech.edu/frontpage/>.
- [49] T. M. Tauris and E. P. J. van den Heuvel, *Formation of the Galactic Millisecond Pulsar Triple System PSR J0337+1715—A Neutron Star with Two Orbiting White Dwarfs*, *Astrophys. J. Lett.* **781** (Jan., 2014) L13, [[arXiv:1401.0941](#)].
- [50] F. Köpp, J. E. Horvath, D. Hadjimichef, C. A. Z. Vasconcellos, and P. O. Hess, *Internal heating mechanisms in neutron stars*, *Int. J. Mod. Phys. D* **32** (2023), no. 07 2350046, [[arXiv:2208.07770](#)].
- [51] R. Fernandez and A. Reisenegger, *Rotochemical heating in millisecond pulsars. Formalism and non-superfluid case*, *Astrophys. J.* **625** (2005) 291–306, [[astro-ph/0502116](#)].
- [52] A. Reisenegger, P. Jofre, R. Fernandez, and E. Kantor, *Rotochemical Heating of Neutron Stars: Rigorous Formalism with Electrostatic Potential Perturbations*, *Astrophys. J.* **653** (2006) 568–572, [[astro-ph/0606322](#)].
- [53] C. Petrovich and A. Reisenegger, *Rotochemical heating in millisecond pulsars: modified Urca reactions with uniform Cooper pairing gaps*, *Astron. Astrophys.* **521** (2010) A77, [[arXiv:0912.2564](#)].
- [54] N. González-Jiménez, C. Petrovich, and A. Reisenegger, *Rotochemical heating of millisecond and classical pulsars with anisotropic and density-dependent superfluid gap models*, *Mon. Not. Roy. Astron. Soc.* **447** (2015) 2073, [[arXiv:1411.6500](#)].
- [55] E. M. Kantor and M. E. Gusakov, *Long-lasting accretion-powered chemical heating of millisecond pulsars*, *MNRAS* **508** (Dec., 2021) 6118–6127, [[arXiv:2110.02881](#)].
- [56] K. Yanagi, N. Nagata, and K. Hamaguchi, *Cooling Theory Faced with Old Warm Neutron Stars: Role of Non-Equilibrium Processes with Proton and Neutron Gaps*, *Mon. Not. Roy. Astron. Soc.* **492** (2020), no. 4 5508–5523, [[arXiv:1904.04667](#)].
- [57] M. E. Gusakov, E. M. Kantor, and A. Reisenegger, *Rotation-induced deep crustal heating of millisecond pulsars*, *MNRAS* **453** (Oct., 2015) L36–L40, [[arXiv:1507.04586](#)].
- [58] P. W. Anderson and N. Itoh, *Pulsar glitches and restlessness as a hard superfluidity phenomenon*, *Nature* **256** (1975) 25–27.
- [59] M. A. Alpar, D. Pines, P. W. Anderson, and J. Shaham, *Vortex creep and the internal temperature of neutron stars. I - General theory*, *APJ* **276** (Jan., 1984) 325–334.
- [60] N. Shibazaki and F. K. Lamb, *Neutron Star Evolution with Internal Heating*, *APJ* **346** (Nov., 1989) 808.
- [61] H. Umeda, N. Shibazaki, K. Nomoto, and S. Tsuruta, *Thermal Evolution of Neutron Stars with Internal Frictional Heating*, *APJ* **408** (May, 1993) 186.
- [62] K. Van Riper, B. Link, and R. Epstein, *Frictional heating and neutron star thermal evolution*, *Astrophys. J.* **448** (1995) 294, [[astro-ph/9404060](#)].
- [63] M. B. Larson and B. Link, *Superfluid friction and late-time thermal evolution of neutron stars*, *Astrophys. J.* **521** (1999) 271, [[astro-ph/9810441](#)].
- [64] P. Goldreich and A. Reisenegger, *Magnetic Field Decay in Isolated Neutron Stars*, *apj* **395** (Aug., 1992) 250.
- [65] G. Baym and D. Pines, *Neutron starquakes and pulsar speedup.*, *Annals of Physics* **66** (Jan., 1971) 816–835.
- [66] M. Baryakhtar et al., *Dark Matter In Extreme Astrophysical Environments, in 2022 Snowmass Summer Study*, 3, 2022. [arXiv:2203.07984](#).

- [67] D. Carney et al., *Snowmass2021 cosmic frontier white paper: Ultraheavy particle dark matter*, *SciPost Phys. Core* **6** (2023) 075, [[arXiv:2203.06508](#)].
- [68] N. Raj, P. Tanedo, and H.-B. Yu, *Neutron stars at the dark matter direct detection frontier*, *Phys. Rev. D* **97** (2018), no. 4 043006, [[arXiv:1707.09442](#)].
- [69] N. F. Bell, G. Busoni, and S. Robles, *Heating up Neutron Stars with Inelastic Dark Matter*, *JCAP* **1809** (2018), no. 09 018, [[arXiv:1807.02840](#)].
- [70] N. F. Bell, G. Busoni, and S. Robles, *Capture of Leptophilic Dark Matter in Neutron Stars*, *JCAP* **1906** (2019), no. 06 054, [[arXiv:1904.09803](#)].
- [71] A. Joglekar, N. Raj, P. Tanedo, and H.-B. Yu, *Relativistic capture of dark matter by electrons in neutron stars*, *Phys. Lett. B* (2020) 135767, [[arXiv:1911.13293](#)].
- [72] A. Joglekar, N. Raj, P. Tanedo, and H.-B. Yu, *Dark kinetic heating of neutron stars from contact interactions with relativistic targets*, *Phys. Rev. D* **102** (2020), no. 12 123002, [[arXiv:2004.09539](#)].
- [73] N. F. Bell, G. Busoni, S. Robles, and M. Virgato, *Improved Treatment of Dark Matter Capture in Neutron Stars II: Leptonic Targets*, *JCAP* **03** (2021) 086, [[arXiv:2010.13257](#)].
- [74] R. Garani and J. Heeck, *Dark Matter Interactions with Muons in Neutron Stars*, *Phys. Rev. D* **100** (2019), no. 3 035039, [[arXiv:1906.10145](#)].
- [75] C.-S. Chen and Y.-H. Lin, *Reheating neutron stars with the annihilation of self-interacting dark matter*, *JHEP* **08** (2018) 069, [[arXiv:1804.03409](#)].
- [76] K. Hamaguchi, N. Nagata, and K. Yanagi, *Dark Matter Heating vs. Rotochemical Heating in Old Neutron Stars*, *Phys. Lett. B* **795** (2019) 484–489, [[arXiv:1905.02991](#)].
- [77] R. Garani, Y. Genolini, and T. Hambye, *New Analysis of Neutron Star Constraints on Asymmetric Dark Matter*, *JCAP* **1905** (2019), no. 05 035, [[arXiv:1812.08773](#)].
- [78] D. A. Camargo, F. S. Queiroz, and R. Sturani, *Detecting Dark Matter with Neutron Star Spectroscopy*, *JCAP* **1909** (2019), no. 09 051, [[arXiv:1901.05474](#)].
- [79] N. F. Bell, G. Busoni, S. Robles, and M. Virgato, *Improved Treatment of Dark Matter Capture in Neutron Stars*, [[arXiv:2004.14888](#)].
- [80] N. F. Bell, G. Busoni, T. F. Motta, S. Robles, A. W. Thomas, and M. Virgato, *Nucleon Structure and Strong Interactions in Dark Matter Capture in Neutron Stars*, [[arXiv:2012.08918](#)].
- [81] F. Anzuini, N. F. Bell, G. Busoni, T. F. Motta, S. Robles, A. W. Thomas, and M. Virgato, *Improved Treatment of Dark Matter Capture in Neutron Stars III: Nucleon and Exotic Targets*, [[arXiv:2108.02525](#)].
- [82] W.-Y. Keung, D. Marfatia, and P.-Y. Tseng, *Heating neutron stars with GeV dark matter*, *JHEP* **07** (2020) 181, [[arXiv:2001.09140](#)].
- [83] B. Dasgupta, A. Gupta, and A. Ray, *Dark matter capture in celestial objects: light mediators, self-interactions, and complementarity with direct detection*, *JCAP* **10** (2020) 023, [[arXiv:2006.10773](#)].
- [84] Y.-P. Zeng, X. Xiao, and W. Wang, *Constraints on pseudo-nambu-goldstone dark matter from direct detection experiment and neutron star reheating temperature*, [[arXiv:2108.11381](#)].
- [85] T. N. Maity and F. S. Queiroz, *Detecting bosonic dark matter with neutron stars*, [[arXiv:2104.02700](#)].
- [86] M. Fujiwara, K. Hamaguchi, N. Nagata, and J. Zheng, *Capture of Electroweak Multiplet Dark Matter in Neutron Stars*, [[arXiv:2204.02238](#)].

- [87] K. Hamaguchi, N. Nagata, and M. E. Ramirez-Quezada, *Neutron Star Heating in Dark Matter Models for the Muon $g - 2$ Discrepancy*, [arXiv:2204.02413](#).
- [88] J. Coffey, D. McKeen, D. E. Morrissey, and N. Raj, *Neutron star observations of pseudoscalar-mediated dark matter*, *Phys. Rev. D* **106** (2022), no. 11 115019, [[arXiv:2207.02221](#)].
- [89] G. Alvarez, A. Joglekar, M. Phoroutan-Mehr, and H.-B. Yu, *Heating Neutron Stars with Inelastic Dark Matter and Relativistic Targets*, [arXiv:2301.08767](#).
- [90] M. Fujiwara, K. Hamaguchi, N. Nagata, and M. E. Ramirez-Quezada, *Vortex Creep Heating vs. Dark Matter Heating in Neutron Stars*, *Phys. Lett.* **848** (2024) 138341, [[arXiv:2309.02633](#)].
- [91] B. Bertoni, A. E. Nelson, and S. Reddy, *Dark Matter Thermalization in Neutron Stars*, *Phys. Rev.* **D88** (2013) 123505, [[arXiv:1309.1721](#)].
- [92] N. F. Bell, G. Busoni, S. Robles, and M. Virgato, *Thermalization and Annihilation of Dark Matter in Neutron Stars*, [arXiv:2312.11892](#).
- [93] C. Kouvaris, *WIMP Annihilation and Cooling of Neutron Stars*, *Phys. Rev.* **D77** (2008) 023006, [[arXiv:0708.2362](#)].
- [94] A. de Lavallaz and M. Fairbairn, *Neutron Stars as Dark Matter Probes*, *Phys. Rev.* **D81** (2010) 123521, [[arXiv:1004.0629](#)].
- [95] J. F. Acevedo, J. Bramante, R. K. Leane, and N. Raj, *Warming Nuclear Pasta with Dark Matter: Kinetic and Annihilation Heating of Neutron Star Crusts*, *JCAP* **03** (2020) 038, [[arXiv:1911.06334](#)].
- [96] S. Chatterjee, R. Garani, R. K. Jain, B. Kanodia, M. S. N. Kumar, and S. K. Vempati, *Faint light of old neutron stars and detectability at the James Webb Space Telescope*, *Phys. Rev. D* **108** (2023), no. 2 L021301, [[arXiv:2205.05048](#)].
- [97] H. Davoudiasl, D. E. Morrissey, K. Sigurdson, and S. Tulin, *Hylogenesis: A Unified Origin for Baryonic Visible Matter and Antibaryonic Dark Matter*, *Phys. Rev. Lett.* **105** (2010) 211304, [[arXiv:1008.2399](#)].
- [98] H. Davoudiasl, D. E. Morrissey, K. Sigurdson, and S. Tulin, *Baryon Destruction by Asymmetric Dark Matter*, *Phys. Rev. D* **84** (2011) 096008, [[arXiv:1106.4320](#)].
- [99] M. Jin and Y. Gao, *Nucleon - Light Dark Matter Annihilation through Baryon Number Violation*, *Phys. Rev. D* **98** (2018), no. 7 075026, [[arXiv:1808.10644](#)].
- [100] A. Herrero, M. A. Pérez-García, J. Silk, and C. Albertus, *Dark matter and bubble nucleation in old neutron stars*, *Phys. Rev. D* **100** (2019), no. 10 103019, [[arXiv:1905.00893](#)].
- [101] Y. Bai, J. Berger, M. Korwar, and N. Orlofsky, *Phenomenology of magnetic black holes with electroweak-symmetric coronas*, *JHEP* **10** (2020) 210, [[arXiv:2007.03703](#)].
- [102] J. Bramante, B. J. Kavanagh, and N. Raj, *Scattering Searches for Dark Matter in Subhalos: Neutron Stars, Cosmic Rays, and Old Rocks*, *Phys. Rev. Lett.* **128** (2022), no. 23 231801, [[arXiv:2109.04582](#)].
- [103] M. I. Gresham, V. S. H. Lee, and K. M. Zurek, *Astrophysical observations of a dark matter-Baryon fifth force*, *JCAP* **02** (2023) 048, [[arXiv:2209.03963](#)].
- [104] D. McKeen, M. Pospelov, and N. Raj, *Cosmological and astrophysical probes of dark baryons*, *Phys. Rev. D* **103** (2021), no. 11 115002, [[arXiv:2012.09865](#)].
- [105] D. McKeen, M. Pospelov, and N. Raj, *Neutron Star Internal Heating Constraints on Mirror Matter*, *Phys. Rev. Lett.* **127** (2021), no. 6 061805, [[arXiv:2105.09951](#)].

- [106] I. Goldman, R. N. Mohapatra, S. Nussinov, and Y. Zhang, *Constraints on neutron-mirror-neutron oscillation from neutron star cooling*, *Eur. Phys. J. C* **82** (2022), no. 10 945, [[arXiv:2203.08473](#)].
- [107] I. Goldman, R. N. Mohapatra, S. Nussinov, and Y. Zhang, *Neutron-Mirror-Neutron Oscillation and Neutron Star Cooling*, *Phys. Rev. Lett.* **129** (2022), no. 6 061103, [[arXiv:2208.03771](#)].
- [108] Z. Berezhiani, R. Biondi, M. Mannarelli, and F. Tonelli, *Neutron-mirror neutron mixing and neutron stars*, *Eur. Phys. J. C* **81** (2021), no. 11 1036, [[arXiv:2012.15233](#)].
- [109] H. Davoudiasl, *Stellar signals of a baryon-number-violating long-range force*, *Phys. Rev. D* **108** (2023), no. 1 015023, [[arXiv:2304.06071](#)].
- [110] Y. Ema, R. McGehee, M. Pospelov, and A. Ray, *Dark Matter Catalyzed Baryon Destruction*, [arXiv:2405.18472](#).
- [111] J. Bramante and N. Raj, *Dark matter in compact stars*, [arXiv:2307.14435](#).
- [112] M. Pato, F. Iocco, and G. Bertone, *Dynamical constraints on the dark matter distribution in the Milky Way*, *JCAP* **12** (2015) 001, [[arXiv:1504.06324](#)].
- [113] R. Garani, A. Gupta, and N. Raj, *Observing the thermalization of dark matter in neutron stars*, *Phys. Rev. D* **103** (2021), no. 4 043019, [[arXiv:2009.10728](#)].
- [114] M. I. Gresham, V. S. H. Lee, and K. M. Zurek, *Astrophysical observations of a dark matter-Baryon fifth force*, *JCAP* **02** (2023) 048, [[arXiv:2209.03963](#)].
- [115] G. D. Illingworth et al., *The HST eXtreme Deep Field (XDF): Combining All ACS and WFC3/IR Data on the HUDF Region into the Deepest Field Ever*, *Astrophys. J. Suppl.* **209** (2013) 6, [[arXiv:1305.1931](#)].